Monitoring of a sludge dewatering equipment by image classification

Sandro Maquiné de Souza[*a], Yves Grandvalet[a], Thierry Denoeux[a]

[a]Université de Technologie de Compiègne, Laboratoire Heudiasyc, B.P. 20529, 60205 Compiègne, France

ABSTRACT

Belt filter presses represent an economical means to dewater the residual sludge generated in wastewater treatment plants. In order to assure maximal water removal, the raw sludge is mixed with a chemical conditioner prior to being fed into the belt filter press. When the conditioner is properly dosed, the sludge acquires a coarse texture, with space between flocs. This information was exploited for the development of a software sensor, where digital images are the input signal, and the output is a numeric value proportional to the dewatered sludge dry content. Three families of features were used to characterize the textures. Gabor filtering, wavelet decomposition and co-occurrence matrix computation were the techniques used. A database of images, ordered by their corresponding dry contents, was used to calibrate the model that calculates the sensor output. The images were separated in groups that correspond to single experimental sessions. With the calibrated model, all images were correctly ranked within an experiment session. The results were very similar regardless of the family of features used. The output can be fed to a control system, or, in the case of fixed experiment conditions, it can be used to directly estimate the dewatered sludge dry content.

Keywords: Gabor filters, co-occurrence matrix, wavelet transform, texture analysis, belt filter press, residual sludge, sludge dewatering, software sensor, wastewater treatment.

1. INTRODUCTION

The European Union Directive concerning urban waste water treatment[6] stated that by the end of 2005, all wastewaters collected in all agglomerations with more than 2000 inhabitants should be subject to a secondary treatment or equivalent (organic matter removal). As a consequence, the quantity of residual sludge generated in the wastewater treatment plants has been growing ever since. In 1992, 5.5 million tonnes of dry matter were produced in the European Community; a production of nearly 9 million tonnes is expected by the end of 2005 in the same geographical area.

Regardless of the final destination of the residual sludge, the reduction of its water content is recommended in order to reduce transportation costs and make further treatments easier. Several equipments can be employed to dewater the sludge: the filter press, the centrifuge, the belt filter press. The choice of the dewatering device depends on some factors like investment costs, desired dry content level, type and quantity of sludge to process.

For small plants, the belt filter press is a good alternative. It allows a continuous treatment of the sludge, with relatively low investment costs and low energy consumption[4, 13, 5]. The sludge is first mixed with a conditioning agent to enhance particle aggregation. In the free drainage zone, some water is removed by gravity draining and the material is then compressed between two tensioned porous belts, generating the dewatered sludge (Fig. 1).

In the present day, there are no economical means to automatically monitor the belt filter press operation. The dry content analysis must be done offline, and other alternatives to this measure (Capillary Suction Time, Specific Resistance to Filtration) do not correlate with the final water content of the treated sludge[16].

In the free drainage zone, the conditioned sludge texture can be observed. A well conditioned sludge will be more dewatered. The texture that corresponds to good conditioning is coarse with space between sludge flocs[15] (Fig. 2). This "visual parameter" is actually used by operators to set up the dewatering device.

[*] maquine@utc.fr, gmaquine@hotmail.com; phone +33 3 4423 4430; fax +33 3 4423 4477

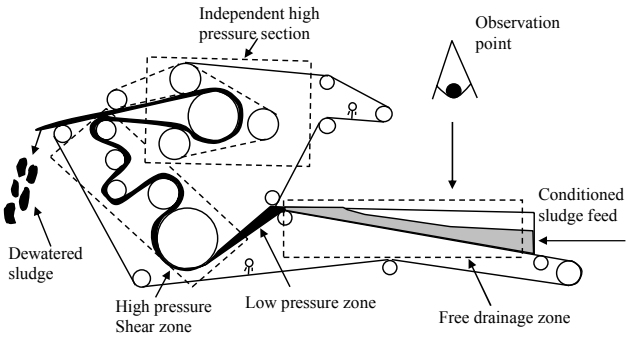

Figure 1. Belt filter press scheme with observation point.

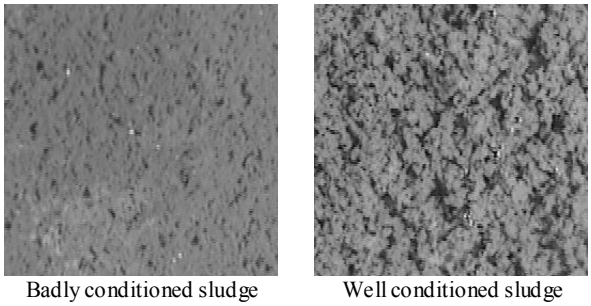

Badly conditioned sludge texture | Well conditioned sludge texture

Figure 2. Conditioned sludge textures. Badly conditioned sludge corresponds to less dewatered sludge thus low dry content; well conditioned sludge corresponds to more dewatered sludge thus high dry content.

The online automatic monitoring of the belt filter press operation would then be possible if there was a system that could recognize "good textures" and "bad textures". Based on this, a new software sensor was conceived: images of the sludge texture constitute the input; the output is an indication of the "quality" of the texture. A good quality texture corresponds to highly dewatered sludge.

This sensor is constituted by the following parts:

- Image acquisition system (digital camera and storage device);
- Feature extraction software (image texture is translated into meaningful numeric values);
- Output calculation (the features are used to calculate the quality of the texture).

The way a control system can use the sensor output is simple: by maximizing this output, the dewatered sludge dry content will also be maximized. The manipulated variable can be, for example, the chemical conditioner flow rate.

To build up the sensor, the following steps were followed:

- Use of a database containing digital images and their corresponding dry content analyses;
- Extraction of useful information from the images: computation of features which are sensible to texture;
- Manual ranking of selected images with respect to their relative dry content;
- Development and calibration of a model that ranks the images with respect to their corresponding dry content;
- Verification that the images were correctly ranked.

The choice of a ranking model, instead of a model that would directly calculate the dry content, is justified by the following reasons:

- The image database is organized in several experimental sessions. From one session to another, the *image acquisition conditions* may vary (position of light source, position of camera, focus) as well as *belt filter press adjustments* (belt tension, belt speed). The former implies in several possible images of the same object (several textures correspond to the same observed sludge portion) and the latter implies in several possible dry content values for the same conditioned sludge. If all images were acquired in the same conditions, a tight relation between texture and dry content could be determined. This is true only for images within a single experimental session;
- The sampling protocol for water content analysis was not mastered during the first sessions; the dry content values are not enough accurate because they do not represent the mean dry content of all the sludge at a given time (the uncertainty is more than 3% dry mass/total mass; an error of less than 1% dry mass/total mass is necessary to determine the quality of the dewatered sludge); accurate dry content values would be necessary to calibrate the model;

- Despite the different experimental conditions in different experimental sessions, the kind of information to be exploited is the same for all of them: coarser textures correspond to higher dry contents, smoother textures correspond to lower dry contents;
- Images from the same session can be ranked by visual inspection, even if dry content estimates are poor;
- Rankings from several sessions can be used together to calibrate the model;
- To maximize the output of the model means to maximize the dewatered sludge dry content, even if these values are unknown.

2. METHODOLOGY

2.1. Image database

The database is organized in 5 groups of images, each one corresponding to a single experimental session. In a group there can be two or three ranks; the higher the rank, the higher the corresponding dry content. Image dimensions are 512 × 512 pixels, which represents a surface of 14.5 cm × 14.5 cm. Each image sample shown in table 1 represents a group of 5 similar images. The total number of images is 70.

Table 1. Image database composed of 70 images grouped by experimental sessions and operator-determined ranks. Each image shown here represents a group of 5 similar images. An increase in texture coarseness can be noticed from top to bottom (ranks 2 and 3 of session 2 are not really distinguishable). DC stands for Dry Content, unit is percent of dry mass over total mass.

Session ⟶		1	2	3	4	5
Rank determined by operator ↓ Increasing roughness	1	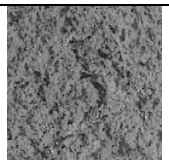 DC = 14.1 %	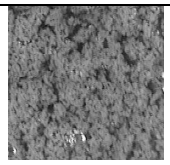 DC = 13.9 %	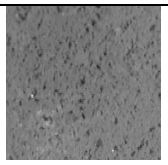 DC = 12.7 %	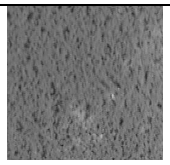 DC = 13.0 %	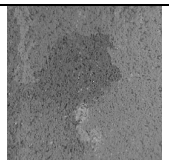 DC = 13.5 %
	2	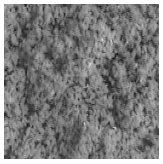 DC = 14.7 %	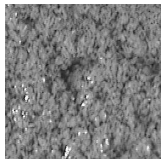 DC = 14.4 %	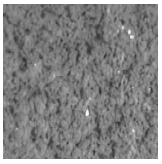 DC = 13.9 %	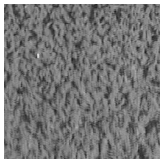 DC = 15.3 %	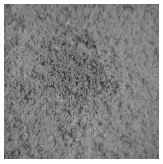 DC = 16.6 %
	3		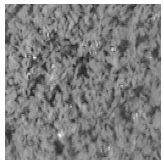 DC =15.5 %	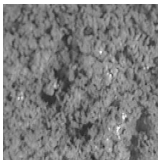 DC = 15.9 %	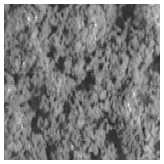 DC = 16.0 %	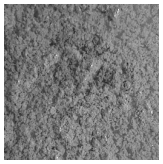 DC = 18.8 %

The ranks are *not* directly linked to dry content values. They are just a simplified way to tell selected textures apart. Dry content values cannot be compared from one session to another in terms of rank number. Images and dry contents should only be compared within the same session, due to the reasons exposed before in this text.

2.2. Feature extraction from images

Three kinds of features which are sensible to texture were calculated from the images. The techniques used were co-occurrence matrix computation[9], Gabor filtering[7], and discrete wavelet decomposition[2]. The first technique was introduced by Haralick[9]and it exploits the distribution of gray levels in the image for a given pair of pixels that are separated by a fixed distance. The co-occurrence matrix is a two-dimensional histogram of the gray levels pointed by both pixels. Some statistical measures calculated from this matrix were used as features. In the case of the other two techniques, the digital image is decomposed into a set of subimages whose frequency band is limited. The energy contained in each one of these subimages was used as a feature.

2.2.1. Gabor features

The image $i(x, y)$, $(x, y) \in \Omega$ (Ω is the set of image points) is convolved with a 2 dimensional Gabor function $g(x, y)$, $(x, y) \in \Omega$ to obtain a Gabor feature image $r(x, y)$. The Gabor function used in the spatial domain is:

$$g(x, y) = \exp\left(-\frac{1}{2}\left(\frac{x'^2}{\sigma_{x'}^2}+\frac{y'^2}{\sigma_{y'}^2}\right)\right)\cos(2\pi f\, x'), \tag{1}$$

where $x' = x\cos\theta + y\sin\theta, y' = -x\sin\theta + y\cos\theta$;
f is the frequency of a sinusoidal plane wave, θ is the anti-clockwise rotation of the Gaussian envelope and the sinusoid, and $\sigma_{x'}$ and $\sigma_{y'}$ are the space constants of the Gaussian envelope along the x' and y' axes, respectively.

The Fourier domain representation of (1) is given by

$$G(u, v) = A\left(\exp\left\{-\frac{1}{2}\left(\frac{(u'-f)^2}{\sigma_{u'}^2}+\frac{v'^2}{\sigma_{v'}^2}\right)\right\}+\exp\left\{-\frac{1}{2}\left(\frac{(u'+f)^2}{\sigma_{u'}^2}+\frac{v'^2}{\sigma_{v'}^2}\right)\right\}\right), \tag{2}$$

where $\sigma_{u'} = 1/(2\pi\sigma_{x'})$, $\sigma_{v'}=1/(2\pi\sigma_{y'})$, $A=2\pi\,\sigma_{x'}\sigma_{y'}$, $u' = u\cos\theta + v\sin\theta$, $v' = -u\sin\theta + v\cos\theta$.

The Gabor filter bank used herewith follows the specifications of Jain & Farrokhnia[11]. Frequencies and orientations used were: $f \in \left\{\sqrt{2}, 2\sqrt{2}, 4\sqrt{2}, ..., 128\sqrt{2}\right\}$, total of 8; $\theta \in \{0°, 45°, 90°, 135°\}$, total of 4.
The feature image R is computed by a convolution in the Fourier domain, an element-wise multiplication:

$$R_{f,\theta}(u,v) = G_{f,\theta}(u,v)\ .\ I(u,v), \tag{3}$$

where $I(u,v)$ is the image represented in the Fourier domain. The total energy of the 2D signal (feature image) is used as a feature:

$$E_{f,\theta} = \sum_{u,v}\left|R_{fo,\theta}(u,v)\right|^2\ . \tag{4}$$

Up to this point we have a total of 32 features. This number can be reduced by combining the energies from the four orientations:

$$E_f = \sum_j E_{f,\theta_j}\ . \tag{5}$$

Finally, the total number of features per image is 8. If this number turns out to be too small (bad classification results), the full set of features can be tested.

2.2.2. Wavelet decomposition features

A wavelet is a waveform of effectively limited duration that has an average value of zero. In wavelet analysis, the signal to be analyzed is compared to a selected set of wavelets. *Scale* and *position* are the new coordinates of the transformed signal.
The continuous wavelet transform for a one dimensional signal is given by:

$$W(scale, position) = \int_{-\infty}^{+\infty} f(x)\psi(scale, position, x)dx\ , \tag{6}$$

where $\psi(scale, position)$ is computed from the mother wavelet ψ by translation and dilation

$$\psi(scale, position) = \frac{1}{\sqrt{scale}}\psi\left(\frac{x - position}{scale}\right) \tag{7}$$

The values $W(scale, position)$ are also called *wavelet coefficients*. *Scale* is the number of times the wavelet is stretched (Fig. 3). *Position* indicates the translation of the wavelet (Fig. 4).

This transformation can be extended to the two-dimensional case. In order to cover all the plane, a rotation parameter is added. In this case the analysis is very similar to the one performed with Gabor filters, especially if the Morlet wavelet is used (Daubechies, 1992).

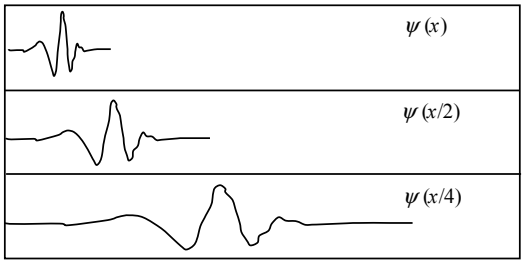

Figure 3. Different scales for the same wavelet function (role of *scale* parameter).

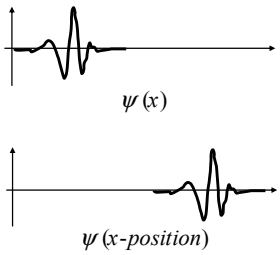

Figure 4. Wavelet function and its shifted version (role of *position* parameter).

Equation (6) can be discretized by restraining *scale* and *position* to a discrete lattice (*scale* = $2^{n \in \mathbb{Z}}$, *position* $\in \mathbb{Z}$). With this base, the analysis is obtained from the *discrete wavelet transform*, also called *pyramidal wavelet decomposition*.

In two dimensions, for a given scale, a set of 3 directions are fixed for the translations: 0°, 45°, 90°. The set of coefficients obtained for a given scale and direction (for all translations) are called *details*. The remaining signal, which is the original subtracted from its details, is called *approximation*. An example of pyramidal decomposition for one of the images of the database is shown in Figure 5.

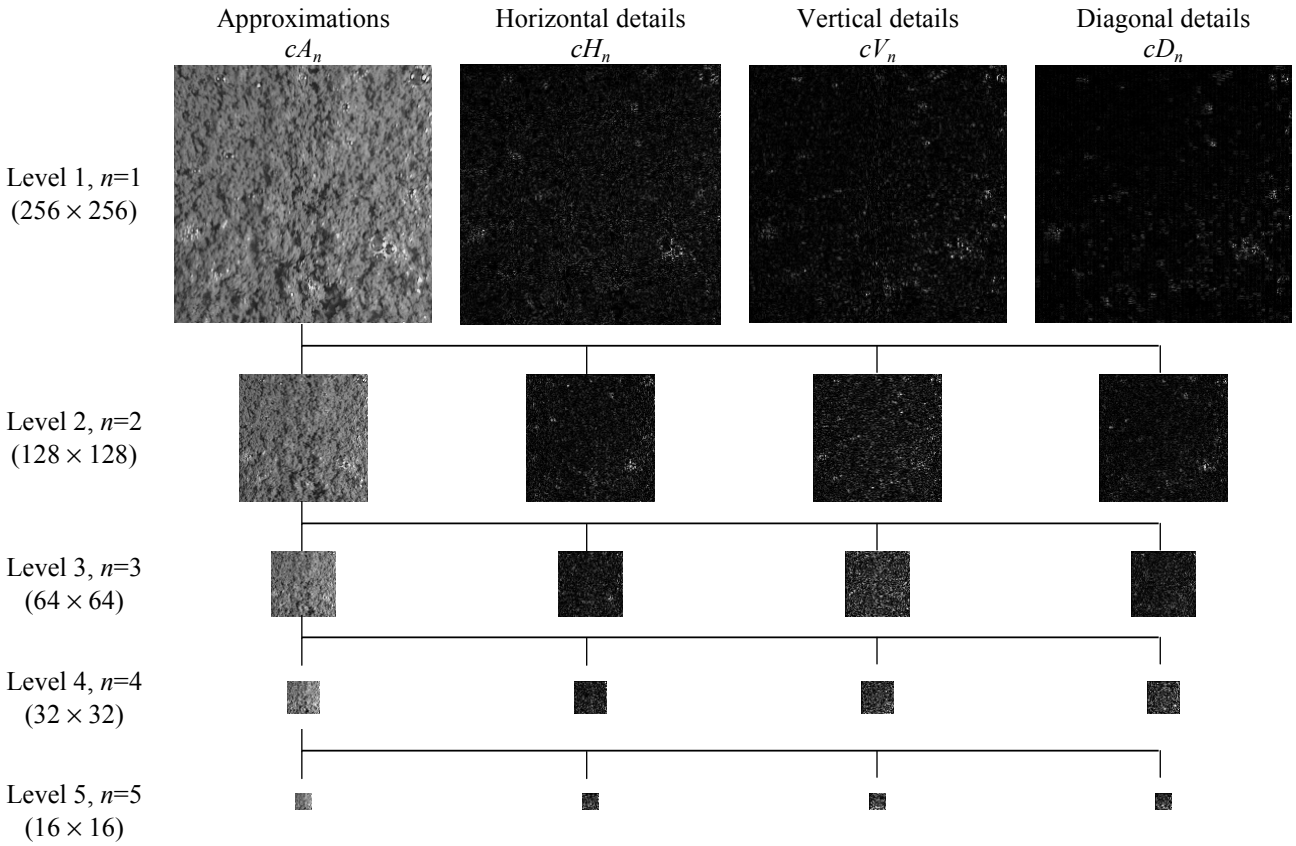

Figure 5. Discrete wavelet coefficients up to level 5. The original image is 512 × 512 pixels. n = level of decomposition (*scale* = 2^n). cA_n = approximation coefficients at level n. cH_n = horizontal details, cV_n = vertical details, cD_n = diagonal details.

Randen and Husøy[17] compared a number of filtering techniques for texture classification. Results were similar for the wavelets tested, and the Daubechies wavelet of 4th order, "db4", provided slightly better results. This wavelet is used in this work.

The energies from the detail coefficients were used as features:

$$eH_n = \frac{2^{(2n)}}{512^2}\sum_{i=1}^{2^{9-n}}\sum_{j=1}^{2^{9-n}}\left(cH_n(i,j)\right)^2 \;;\; eV_n = \frac{2^{(2n)}}{512^2}\sum_{i=1}^{2^{9-n}}\sum_{j=1}^{2^{9-n}}\left(cV_n(i,j)\right)^2 \;;\; eD_n = \frac{2^{(2n)}}{512^2}\sum_{i=1}^{2^{9-n}}\sum_{j=1}^{2^{9-n}}\left(cD_n(i,j)\right)^2 . \quad (8)$$

$$\underline{W} = [eH_1, eV_1, eD_1, eH_2, eV_2, eD_2, \ldots, eH_5, eV_5, eD_5], \quad (9)$$

where $\underline{W}$ is the feature vector. The total number of wavelet features is 15.

2.2.3. Co-occurrence matrix features

A co-occurrence matrix is a square matrix with elements corresponding to relative frequency of pairs of gray levels of pixels separated by a certain distance in a given direction. Haralick[9] proposed 14 measures of textural features which are derived from the co-occurrence matrix. Four features commonly used[9, 14] were selected for this work. They are the Angular Second Moment (ASM), Contrast (Con), Correlation (Cor) and Entropy (Ent). They are given by the following expressions ($\underline{C}$ is the co-occurrence matrix):

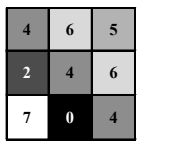

a \ b	0	1	2	3	4	5	6	7
0	0	0	0	0	0	0	0	0
1	0	0	0	0	0	0	0	0
2	1	0	0	0	0	0	0	0
3	0	0	0	0	0	0	0	0
4	0	0	0	0	2	0	0	0
5	0	0	0	0	0	0	0	0
6	0	0	0	0	0	0	1	0
7	0	0	0	0	0	0	0	0

Resulting co-occurrence matrix

Figure 6. Co-occurrence matrix for a small gray-level image. *a* is the gray level of the starting pixel and *b* is the gray level of the pixel pointed by the translation vector.

$$ASM = \frac{1}{p^2}\sum_i\sum_j (C(i,j))^2 , \quad (10)$$

$$Con = \frac{1}{p\cdot(G-1)^2}\sum_{k=0}^{G-1} k^2 \sum_{|i-j|=k} C(i,j) , \quad (11)$$

$$Cor = \frac{1}{p\cdot\sigma_x\cdot\sigma_y}\sum_i\sum_j (i-\mu_x)\cdot(j-\mu_y)\cdot C(i,j) , \text{ and} \quad (12)$$

$$Ent = 1 - \frac{1}{p\cdot \mathrm{Ln}(p)}\sum_i\sum_j C(i,j)\cdot \mathrm{Ln}^*(C(i,j)) . \quad (13)$$

where G is the number of gray levels; p is the number of pairs: $p = \sum_i\sum_j C(i,j)$;

$\mathrm{Ln}^*(C(i,j)) = \begin{cases} \mathrm{Ln}\,(C(i,j)), \text{if } C(i,j) \neq 0 \\ 0, \text{otherwise} \end{cases}$; $\mu_x = \frac{1}{p}\sum_i\sum_j i\cdot C(i,j)$; $\mu_y = \frac{1}{p}\sum_i\sum_j j\cdot C(i,j)$;

$\sigma_x^2 = \frac{1}{p}\sum_i\sum_j (i-\mu_x)^2\cdot C(i,j)$, and $\sigma_y^2 = \frac{1}{p}\sum_i\sum_j (j-\mu_y)^2\cdot C(i,j)$. The features above are normalized as described by Cocquerez and Philipp[1].

The original 256-gray-level images were converted to 32-gray-level images for the co-occurrence matrix computation (G=32). Nearest neighbor pairs of pixels at orientations 0°, 45°, 90° and 135° were used, as suggested by Ohanian[14] and Strand[18]. The total number of co-occurrence matrix features is 16.

2.3. Model for ordinal regression

The ranking technique based on the margin concept of support vector machines (SVMs)[19] proposed by Herbrich *et al.*[10] was used to extract features from the pairwise image comparisons.

Let $\underline{x}$ be the feature vector of an image: $\underline{x} = [x_1, x_2, ..., x_d]^{\mathrm{T}}$, (14)

where d is the total number of features.

The model output $y(\underline{x})$ is a real scalar value, the rank of the image:

$$\begin{cases} y(\underline{x}) = \underline{w}^T \underline{x} \\ \underline{w} = [w_1, w_2, ..., w_d]^T \end{cases} \tag{15}$$

where $\underline{w}$ is the parameter vector of the model.

For every pair of images, ordered with respect to their corresponding dry contents: $\mathrm{Image_i} \succ \mathrm{Image_j}$; $i, j \in \{1, 2, ..., n\}$,

where n = total number of images, the model should ensure that: $y(\underline{x}_i) > y(\underline{x}_j) \Rightarrow \underline{w}^T \underline{x}_i > \underline{w}^T \underline{x}_j$, (16)

and an arbitrary separation between ranks should be chosen. We choose this value to be 1:

$$\underline{w}^T \underline{x}_i \geq \underline{w}^T \underline{x}_j + 1. \tag{17}$$

Let $\underline{\underline{R}}$ be the logical matrix of ordered pairs of images (lower triangular matrix):

$$\underline{\underline{R}} = \left[\begin{array}{c|cccc} & j=1 & j=2 & ... & j=n \\ \hline i=1 & 0 & 0 & ... & 0 \\ i=2 & R(2,1) & 0 & ... & 0 \\ ... & ... & ... & ... & ... \\ i=n & R(n,1) & R(n,2) & ... & 0 \end{array}\right] \tag{18}$$

$$R(i,j) = \begin{cases} 1, \text{if } \mathrm{Image_i} \succ \mathrm{Image_j} \\ 0, \text{otherwise} \end{cases}$$

Let $\underline{I}$ and $\underline{J}$ be the vectors of indices of $\underline{\underline{R}}$ where $R(i,j) = 1$, $i \in \underline{I}$ and $j \in \underline{J}$: $\underline{I} = [i_1, i_2, \ldots, i_m]$, $\underline{J} = [j_1, j_2, \ldots, j_m]$, where m = total number of ordered pairs, $m = \sum_{i;j} R(i,j)$.

The optimization problem can be written as follows:

$$\begin{aligned} &\min_{\underline{w}} \frac{1}{2}\|\underline{w}\|^2, \text{subject to } \underline{w}^T(\underline{x}_{I_k} - \underline{x}_{J_k}) \geq 1 \\ &\forall k \in \{1,2,...,m\} \end{aligned} \tag{19}$$

In order to take model imperfections into account (badly determined ranks or incompatible orderings from different experimental sessions), a slack variable is introduced for every constraint equation. These slack variables should be as small as possible, and non-negative. The optimization problem is then rewritten as follows:

$$\begin{aligned} &\min_{\underline{w},\underline{\xi}} \left\{ \frac{1}{2}\|\underline{w}\|^2 + c\sum_{k=1}^{m} \xi_k \right\}, \text{subject to} \begin{cases} \underline{w}^T(\underline{x}_{I_k} - \underline{x}_{J_k}) \geq 1 - \xi_k \\ \xi_k \geq 0 \end{cases} \\ &\forall k \in \{1, 2, ..., m\} \end{aligned} \tag{20}$$

In the optimization problem (20), in addition to the new parameters to estimate (slack variables, vector $\underline{\xi}$), the value of the hyperparameter c should also be chosen. This can be done by cross-validation.

The problem is solved by a quadratic programming algorithm similar to the one described in Gill and Murray (1981): the routine *quadprog* from Matlab® optimization toolbox.

3. RESULTS

3.1. Determination of the hyperparameter *c*

To determine the hyperparameter *c*, a cross-validation was performed. One optimization is done per experimental session. In each one of these optimizations, data from 4 experimental sessions are used. For the excluded session, we compute a vector of slack variables, $\underline{\xi}^{(E)}$, by (21):

$$\underline{\xi}^{(E)} = \underline{1} - \begin{bmatrix} \underline{w}^T(\underline{x}_{i_1} - \underline{x}_{j_1}) \\ \dots \\ \underline{w}^T(\underline{x}_{i_e} - \underline{x}_{j_e}) \end{bmatrix} \qquad (21)$$

$$s = \sum_{i=1}^{e} \begin{Bmatrix} 1, \text{if } \xi_i^{(E)} > 0 \\ 0, \text{otherwise} \end{Bmatrix} \qquad (22)$$

where *e* is the number of ordered pairs for the excluded session, $e < m$. The number of positive values of $\underline{\xi}^{(E)}$, *s*, is used to evaluate the choice of *c*.

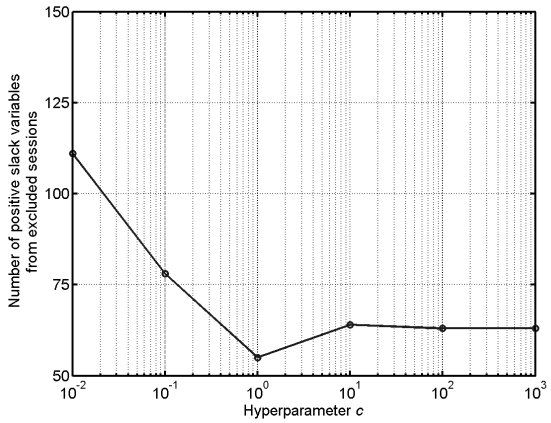

Figure 7. Choice of hyperparameter *c* for the model calibration based on co-occurrence matrix features ($c = 1$).

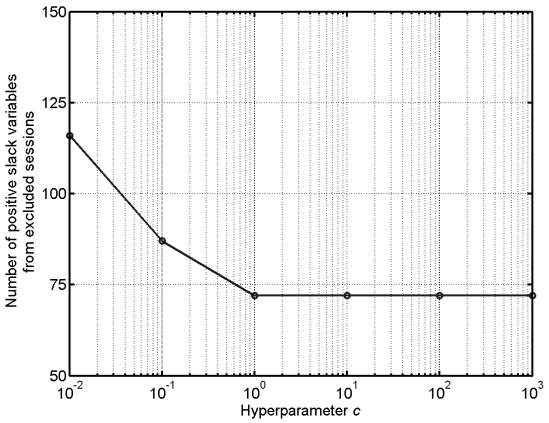

Figure 8. Choice of hyperparameter *c* for the model calibration based on wavelet features ($c = 1$).

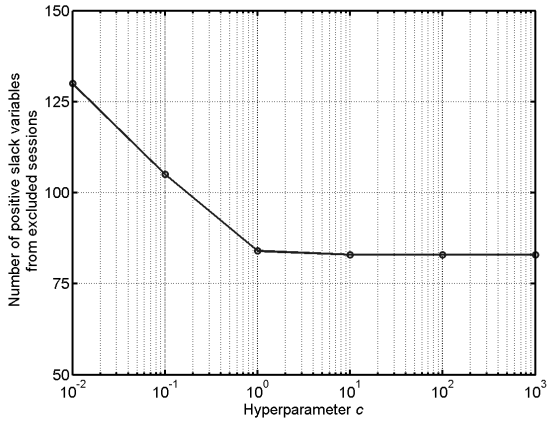

Figure 9. Choice of hyperparameter *c* for the model calibration based on Gabor features ($c = 10$).

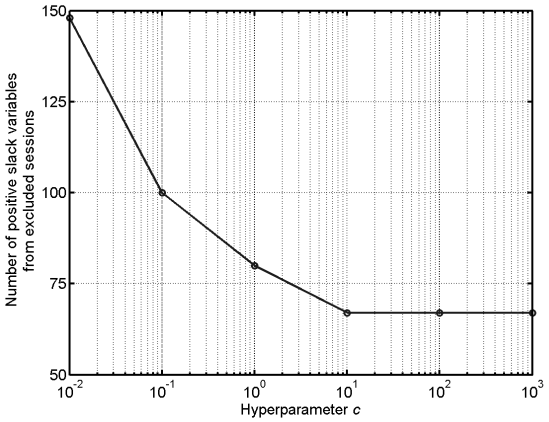

Figure 10. Choice of hyperparameter *c* for the model calibration based on all features ($c = 10$).

In the following sections, results are presented as plots of model output versus operator-determined ranks or dry content values. Each symbol (◂ , ▾ or ▸) corresponds to a single image.

3.2. Results using wavelet features

In Figure 11, manually determined ranks are plotted against model outputs for all the images in the database. Vector $\underline{x}$ contains wavelet analysis-based features. The value c=1 was used, as suggested in figure 8. Features from images from all the experimental sessions were used to calibrate the model. This simple model with 15 linear parameters is able to order all images correctly. The minimum gap between two images from different manual ranks in terms of model output is very near to 1. This indicates that all slack variables are small, so the rankings from different sessions are compatible.

In Figure 12, dry content values are plotted against model output. Not all the curves superpose; this is due to different experimental conditions from one session to another during the image acquisition process, as explained in section 1. Before the last session was carried out, the dewatering process had been enhanced by the operator (several settings had been verified). Therefore, higher dry content values were obtained.

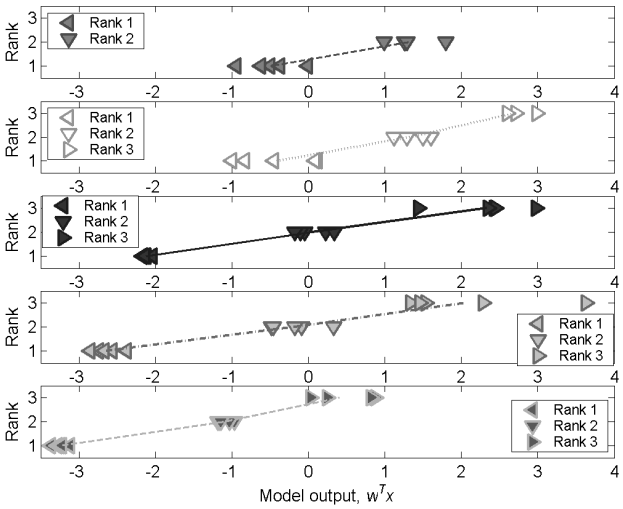

Figure 11. Model response versus manually determined ranks for all experimental sessions. Wavelet-based feature vectors were used.

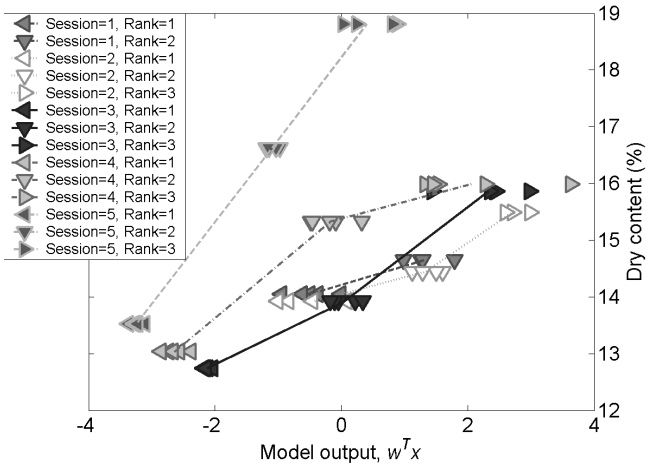

Figure 12. Model responses versus available dry content values for all experimental sessions. Indicated ranks are manually determined ranks. Model is computed from on wavelet-based feature vectors.

3.3. Results using all features

The concatenation of all features would yield a 39-element new set of features. In order to simplify the optimization, the dimensionalities of the feature sets were reduced by principal component analysis (see Jolliffe[17] for more detail on this subject). Each set of features was reduced to a three-element set of features, and these were combined to give a 9-element feature set.

Let $\underline{x}^C$ be the co-occurrence-matrix-based feature vector of an image; similarly, $\underline{x}^W$ is the wavelet-based feature vector of an image and $\underline{x}^G$ is the Gabor-based feature vector of an image. The corresponding matrices of principal components are $\underline{\underline{P}}^C$, $\underline{\underline{P}}^W$, and $\underline{\underline{P}}^G$, computed from the feature vectors of all images in the database, where the first principal component is the first column, the second principal component is the second column, and so on. The new feature vectors ($\underline{x}^{C'}$, $\underline{x}^{W'}$, and $\underline{x}^{G'}$) are computed as follows:

$$\underline{x}^{C'}_{(1\times16)} = \underline{x}^{C}_{(1\times16)} \times \underline{\underline{P}}^{C}_{(16\times16)} \tag{23}$$

$$\underline{x}^{W'}_{(1\times15)} = \underline{x}^{W}_{(1\times15)} \times \underline{\underline{P}}^{W}_{(15\times15)} \tag{24}$$

$$\underline{x}^{G'}_{(1\times8)} = \underline{x}^{G}_{(1\times8)} \times \underline{\underline{P}}^{G}_{(8\times8)} \tag{25}$$

The first three elements of each are concatenated to give a new feature vector, $\underline{x}^{All}$:

$$\underline{x}^{All}_{(1\times9)} = [x_1^{W'} x_2^{W'} x_3^{W'} x_1^{C'} x_2^{C'} x_3^{C'} x_1^{G'} x_2^{G'} x_3^{G'}] \tag{26}$$

The new feature vectors were used to calibrate the model. Results can be seen in figures 13 and 14.

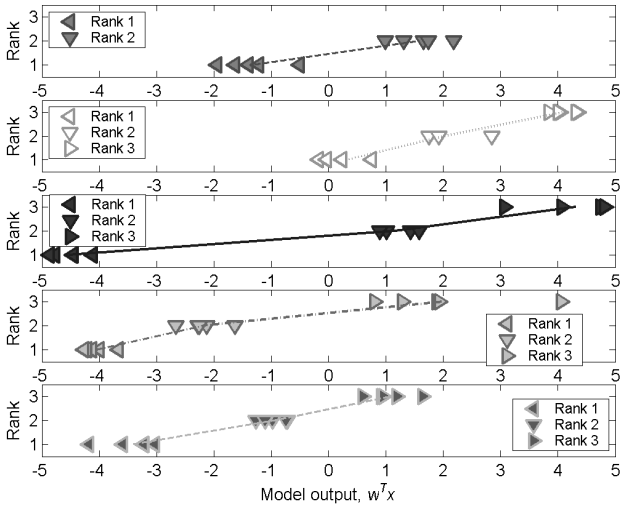

Figure 13. Model response versus manually determined ranks for all experimental sessions. Combined feature vectors were used.

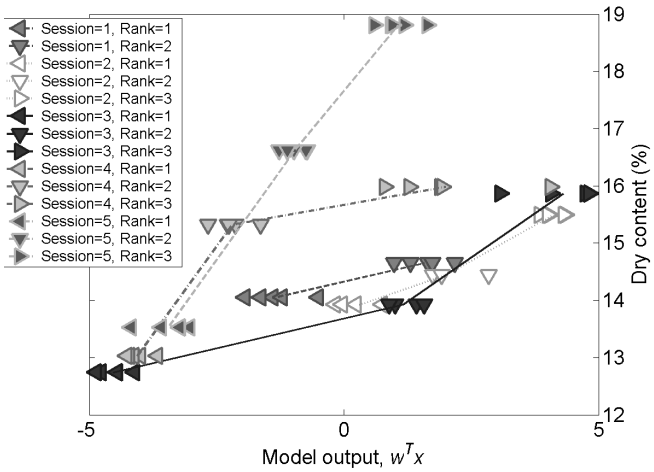

Figure 14. Model responses versus available dry content values for all experimental sessions. Indicated ranks are manually determined ranks. Model is computed from combined feature vectors.

3.4. Discussion

According to Figures 7-10, the best descriptors, in descending order, are: co-occurrence matrix features, all features, wavelet features, and Gabor features.

More wavelet features can be added by implementing *wavelet packet decomposition,* where the detail images are also split. Then a subset of wavelet features can be selected (by principal component analysis, for example) to avoid an excessively high number of features. The same can be done with Gabor features, where the information on the orientations may be restored. A compromise must be reached between number of features and quality of results.

For the prediction of dry content values, the experimental conditions should be stable, as discussed before. It can be seen in figures 12 and 14 that the curves do not superpose. The model output can however be used in a control scheme that would manipulate system variables in order to maximize this output, and hence, maximize dewatered sludge dry content.

In Figure 15, historical data (polymer valve opening and dry content) and model output from session 4 are plotted against time. Model output was computed for all images, even when the acquisition conditions were not stable. For example, the belt fiter press was stopped for the collection of dewatered sludge samples. The model outputs very low values when belt images are inputted to the sensor (without any sludge) as shown in Figure 16. For control systems, this kind of information is important.

Maximum model output corresponds to maximum dry content and vice versa, for all sessions. It can be noticed in Figures 15 and 16 that when polymer dosage is too high, the dry content drops below its maximum value.

4.CONCLUSIONS

Belt filter presses are widely used to remove water from the residual sludge generated in wastewater treatment plants. Their proper operation requires considerable human intervention for maintenance and control.

In this work, a new software sensor has been proposed, which outputs a signal correlated with the dewatered sludge dry content. The input signals are images gathered from a particular point of the belt filter press.

A database composed of digital images and dry content values was used to calibrate a model, whose output, the rank, is an indirect measure of the dewatered sludge dry content.

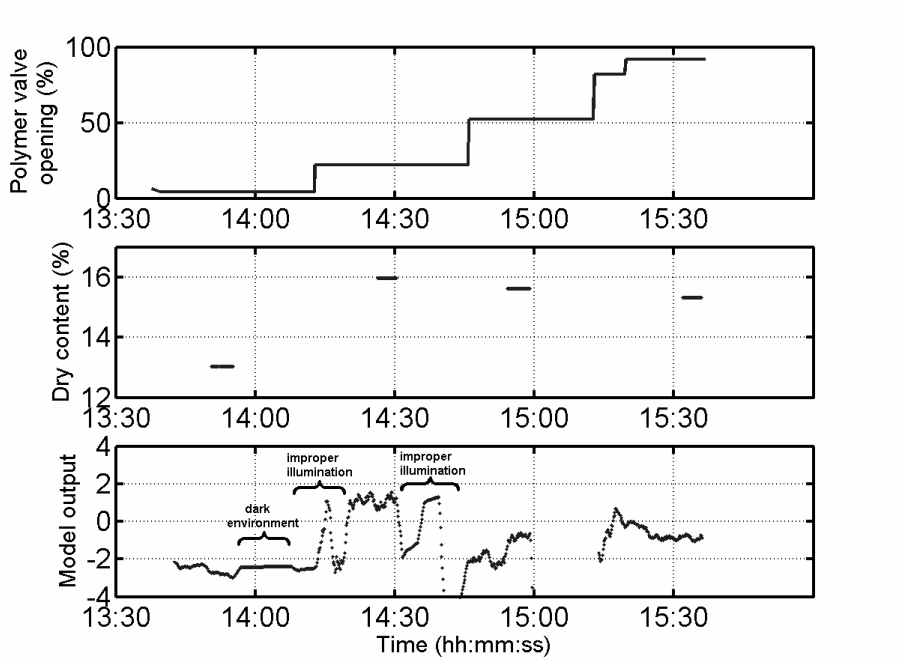

Figure 15. Experimental session number 4. Historical data (polymer valve opening, dry content) and model response. Model based on wavelet features.

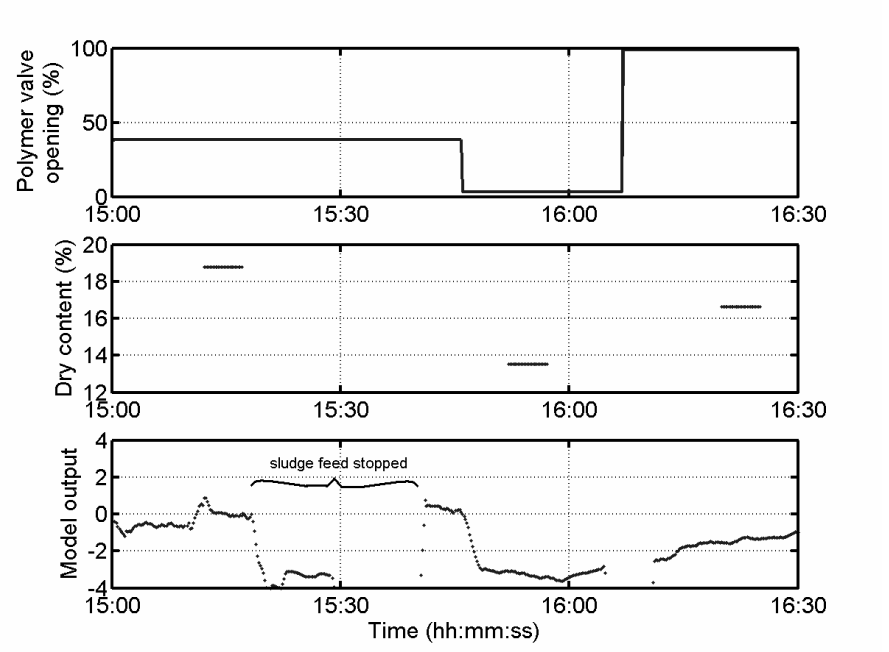

Figure 16. Experimental session number 5. Historical data (polymer valve opening, dry content) and model response. Model based on wavelet features.

To calibrate the model, no dry content values were directly used; instead, some pairs of images were manually ranked in terms of their corresponding dry content values. These images were ranked with regard to their texture (fine or coarse). Conditioned sludge texture constitutes key information used by operators to control the belt filter press.

A number of features were calculated from the digital images. These features are of three types: statistics from gray-level co-occurrence matrices, energies from images that were processed by a Gabor filter bank, and energies from subimages computed from a discrete wavelet decomposition up to the fifth level. Several combinations of features were tested as input to the classification model whose output is linked to the dry content of the dewatered sludge.

The best results are obtained when co-occurrence matrix features are fed to the model, but there is a good correlation between the model output and the available dry content values when other features are used too. The model output can be used as an input to belt filter press control systems.

ACKNOWLEDGEMENTS

We would like to thank *Lyonnaise des Eaux France* for giving access to the wastewater treatment plant where data were acquired. Thanks to *CNPq* (Brazilian National Research Council) for the financial support to Sandro Maquiné for the preparation of his PhD thesis. Thanks to *Université de Technologie de Compiègne* for the financial support to the data acquisition process.

REFERENCES

1. Cocquerez, J.-P. and Philipp, S. *Analyse d'images: filtrage et segmentation*. Masson, Paris, 1995.
2. Daubechies, I. "The wavelet transform, time-frequency localization and signal analysis". *IEEE Transactions on Information Theory*, **36** (5), 961–1005, 1990.
3. Daubechies, I. *Ten lectures on wavelets*. Society for Industrial and Applied Mathematics. Philadelphia, 1992.
4. Dembitz, A.E. "Belt filter presses: a new solution to dewatering?", *Water Environment and Technology*, **15**, 36-42, 1978.
5. Deutsh N.D. "Options in belt filter press". *Water Engineering and Management*, **134** (9), 34-37, 1987.
6. European Union. "Council Directive of 21 May 1991 concerning urban waste water treatment (91/271/EEC)". *Official Journal of the European Union*, L 135, 30.05.1991, p. 40. Luxembourg, 1991.
7. Gabor, D. "Theory of communications". *Journal of the Institution of Electrical Engineers (London)*, **93**, Part III, No. 26, pp 429-457, 1946.
8. Gill, P. E. and W. Murray, and M.H. Wright. *Practical Optimization*, Academic Press, London, 1981.
9. Haralick, R., Shanmugam K. and Dinstein, I. "Texture features for image classification". *IEEE Trans. Syst. Man Cybernet*, **3**, pp. 610–621, 1973.
10. Herbrich, R., Graepel, T. and Obermayer, K. "Large Margin Rank Boundaries for Ordinal Regression". In *Advances in Large Margin Classifiers*, pages 115-132, 2000.
11. Jain, A.K. and Farrokhnia, F. "Unsupervised texture segmentation using Gabor filters". *Pattern Recognition*, **24**, 1167-1186, 1991.
12. Jolliffe, I.T. *Principal Component Analysis*. Springer-Verlag, New York, 1986.
13. Lecey R.W., Pietila, K.A. "Improving belt-filter-press performance". *Chemical Engineering*, **28**, 69-72, 1983.
14. Ohanian, P.P. and Dubes, R.C. "Performance Evaluation for Four Classes of Textural Features". *Pattern Recognition*, **25** (8), pp. 819-833, 1992.
15. OTV. *Traiter et valoriser les boues*, pp. 217-225, Infinités Communication, Rennemoulin (France), 1997.
16. Pan, J.R., Huang, C., Chernga M., Lib, K.-C. and Linb, C.F. "Correlation between dewatering index and dewatering performance of three mechanical dewatering devices". *Advances in Environmental Research*, **7**, 599-602, 2003.
17. Randen, T. and Husøy, J.H. "Filtering for Texture Classification: A Comparative Study". *IEEE Transactions on Pattern Analysis and Machine Intelligence*, **21** (4), pp. 291-310, 1999.
18. Strand, J. and Taxt, T. "Local frequency features for texture classification". *Pattern Recognition*, **27** (10), pp. 1397-1406, 1994.
19. Vapnik, V. N. *The nature of statistical learning theory*. Springer, New York (USA), 1995.